Interactions between Crystalline and Amorphous Domains in Semicrystalline Polymers: Small-Angle X-ray Scattering Studies of the Brill Transition in Nylon 6,6

N. Sanjeeva Murthy*

Research and Technology, AlliedSignal Inc., P.O. Box 1021, Morristown, New Jersey 07962-1021

Zhi-Gang Wang and Benjamin S. Hsiao*

Department of Chemistry, State University of New York at Stony Brook, Stony Brook, New York 11794-3400

Received March 31, 1999; Revised Manuscript Received June 23, 1999

ABSTRACT: The lamellar structures in nylon 6,6 were characterized at several temperatures using synchrotron small-angle X-ray scattering (SAXS) to monitor the changes during the Brill transition at ~160 °C (T_B). The integrated intensity and the coherence length of the lamellar stacks increase during heating above T_B. In contrast, during cooling, the intensity increases below T_B whereas the coherence length increases up to T_B and remains unchanged upon further cooling. The increase in SAXS intensity observed above T_B during heating is attributed to the enhanced contrast resulting from a decrease in the packing density of the amorphous chain segments. It is suggested that the changes in the packing of the crystalline stems, as they do occur during crystalline phase transitions, provoke a proportionate response in the packing of the amorphous chain segments in the interlamellar regions. The thermal expansion coefficient of the amorphous segments calculated from the X-ray diffraction data above T_B is 5.9×10^{-4}/K (molar thermal expansion coefficient, 854×10^{-10} m^3/(mol K)), and this is in reasonable agreement with the published values.

Introduction

Semicrystalline polymers are typically represented as crystalline domains dispersed in an amorphous matrix. Properties of these crystallizable polymers are usually related to percent crystallinity and to the crystalline features such as size and perfection of the crystals. Studies of nylon, polyethylene, and poly(ethylene terephthalate) fibers have shown that orientation and other characteristics of the noncrystalline or amorphous phase also influence the polymer performance.[1−8] In addition, interactions between the crystalline and amorphous regions are also expected to significantly affect the polymer properties.[6−13] Connectivity between the crystalline stems and the amorphous chain segments is often invoked to explain the correlation between lamellar spacings and unit cell dimensions[14] and the decrease in the unit cell volume of the crystals within the lamellae as the amorphous regions swell when exposed to moisture.[15] Such linkages between the amorphous and the crystalline chain segments suggest that changes in the crystalline structure within the lamellae should bring about corresponding changes in the interlamellar regions. We here examine this possibility by following the well-known Brill transition in nylon 6,6 (N66) using small-angle X-ray scattering (SAXS).

During the Brill transition in N66, the room temperature triclinic phase is gradually replaced by a high-temperature pseudohexagonal phase,[16−18] later identified as another triclinic phase of N66.[19] This phenomenon has been investigated by XRD,[16,18−24] DSC,[23−25] NMR,[19,20] and IR.[21,26] In wide-angle X-ray diffraction (WAXD) patterns, at the Brill transition temperature (T_B) two intense reflections, (100) and (010) + (110), associated with the room-temperature triclinic structure of the polymer coalesce into a single reflection. This single reflection persists until the polymer melts, at which point the entire reflection is replaced by an amorphous halo. The transition is very broad, covering a temperature range from about 120 to 180 °C. During this crystalline phase transition, the distance between the H-bonded chains decreases and that between chains bonded by van der Waals interaction, i.e., hydrogen-bonded sheets, increases. We investigate here the influence of this rearrangement of the crystalline stems on the packing of the amorphous chain segments.

Our earlier small-angle neutron scattering data obtained at various temperatures from nylon 6 in the presence of water (D_2O) suggested that crystalline relaxation that brings about structural transformations at T_B could also change the organization of the lamellae.[27] Although the T_B of nylon 6 is 160 °C, these changes occurred at 120 °C. We suspect that this shift to lower temperature is due to water, which is a plasticizer for nylons. Because the polymer began to hydrolyze above 150 °C, there is the possibility that the changes we noticed at 120 °C are perhaps similar to the premelting changes in the lamellar structure reported for other polymers.[28−30] Therefore, here we carried out measurements in the absence of water and on a different nylon. We chose N66 for which the T_B is farther below the melting point than in nylon 6 (nylon 6 melts at 220 °C and N66 at 260 °C although T_B is about 160 °C for both nylons)[20] so that changes other than premelting transitions can be monitored. In this report, we use small-angle X-ray scattering (SAXS) measurements from N66 to show that structural changes in the

* Corresponding authors: phone (973) 455-3764; Fax (973) 455-5295; E-mail nsmurthy@alliedsignal.com.

10.1021/ma990475e CCC: $18.00
Published on Web 07/28/1999

crystalline phase that occur during the Brill transition will affect the amorphous regions.

Experimental Section

Data were collected on the Advanced Polymers beam line (X27C) at the National Synchrotron Light Source (NSLS), Brookhaven National Laboratory, using 1.307 Å wavelength X-rays. The sample-to-detector distance was set at 1903 mm, and the detector resolution was 395 μm. The zero angle and the sample-to-detector distance were determined using the diffraction pattern of a silver behenate standard.

Pellets of Zytel 101 (DuPont) were freeze-milled at liquid nitrogen temperature to a fine powder. The sample was sandwiched between two Kapton films in a 0.7 mm diameter hole in a 1 mm thick copper bar. The sample was first heated to 260 °C, held there for about 15 min, and cooled to ambient temperature (22 °C). This was the starting sample. Data were collected for 10 min as the sample was heated to various preset temperatures up to the melt (260 °C) and then cooled to various preset temperatures. Both wide- and small-angle data were collected simultaneously.

SAXS Data Analysis

The observed scattered intensity in small-angle scattering (SAS) can be directly fitted to the intensity calculated from a suitable model to refine the model parameters.[31−33] We will here use a simple six-parameter model that can be easily implemented using any of the commercially available software packages (we used PeakFit from Jandel).[27] This model is able to account for many of the SAS patterns obtained in the angular range of $0.01 < q < 0.2$, $q = (4\pi \sin \theta)/\lambda$, 2θ being the scattering angle and λ the wavelength. The observed intensity is written as

$$I = I_B + I_D + I_L \quad (1)$$

where I_B is the incoherent background which also takes into account the air scattering, parasitic scattering, etc.; and I_D represents the diffuse scattering with a maximum near the origin (Figure 1). The source of I_D is uncertain and could be due to aggregates of lamellae, microvoids, and domains that scatter as independent entities. No attempt is made here to identify the precise nature of I_D, which varies with the smallest q value in the data. I_L is the scattering from the lamellae and arises from periodic fluctuations in electron density due to alternating crystalline and amorphous regions. The lamellar structures we are analyzing here are essentially one-dimensional structures and hence can be represented as step functions of width $2w$. The Fourier transform of this one-dimensional function is given by

$$F_{step}(w) = \sin(wq)/(wq) \quad (2)$$

Although scattering from a randomly oriented 3-D object can be expressed as a series of Guinier functions, we will assume that the independent scatterers are also one-dimensional structures and their intensity can be written as

$$I_D(q) = [a_1 F_{step}(a_2)]^2 \quad (3)$$

where a_1 is the intensity related to the volume fraction of the independent scatterers, and a_2 is the half-width of the nonperiodic structures with a maximum at $q = 0$ Å^{-1}.

The lamellar peak arises from a periodic lamellar structure, which is a convolution of single lamellae and a lattice function. Thus, the intensity is a product of the Fourier transforms of the lamellar structure factor and the lattice function. The lattice function can be represented as a series of Gaussian peaks, two being sufficient in the angular range of our data. Thus, the intensity I_L of the lamellar peak can be written as

$$I_L(q) = [F_{step}(a_3)\{\text{Gauss}(a_4,a_5,a_6) + \text{Gauss}(a_4,2a_5,a_6)\}]^2/q^2 \quad (4)$$

where

$$\text{Gauss}(a_4,a_5,a_6) = a_4 \exp[-0.5((q - a_5)/a_6)^2] \quad (5)$$

q^2 is the Lorentz factor because the observed $I_L(q)$ is the radial average of the intensity from stacks of lamellar disks; $2a_3$ is the thickness of the interlamellar amorphous layer between the lamellae in the lamellar stack; $F_{step}(a_3)$ is the structure factor of the lamella. Gauss(a_4,a_5,a_6) and Gauss(a_4,$2a_5$,a_6) are the first- and second-order interference functions, respectively. The parameters a_4, a_5, and a_6 are respectively the height, position, and width of the Gaussian peak that represents lamellar reflection. a_4 represents the lamellar intensity. a_5 and a_6 represent the lamellar spacing (L) and coherence length of the lamellar stack (L_{coh}), respectively, and are given by

$$L = 2\pi/a_5 \quad (6)$$

$$L_{coh} = 4\pi/[a_6\sqrt{(8 \ln 2)}] \quad (7)$$

The integrated intensity of the lamellar peak can be calculated from eqs 4 and 5 using the fitted parameters a_3−a_6 and using the standard expression for the area

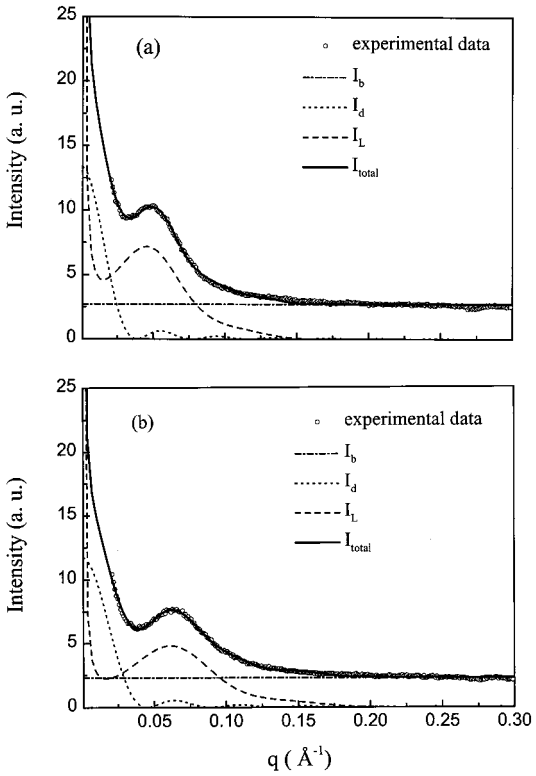

Figure 1. Observed SAXS intensity curve from nylon 6,6 separated into three components: I_B, I_D, and I_L. (a) Data obtained at 200 °C during heating. (b) Data obtained at 40 °C during cooling.

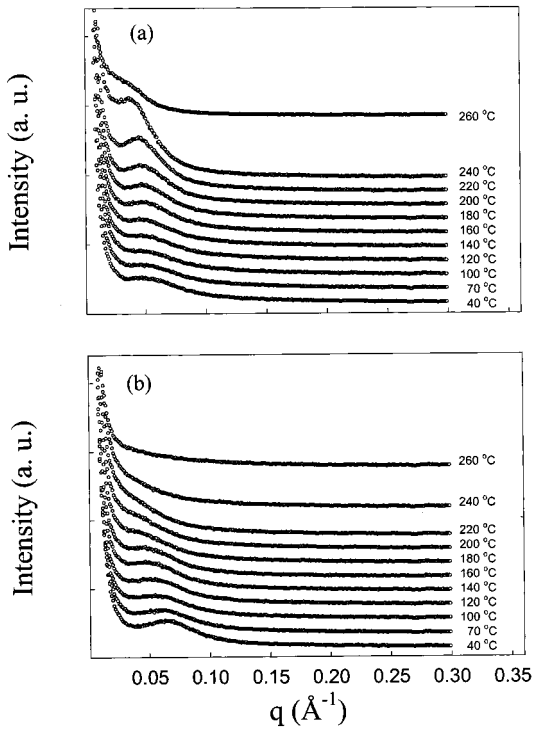

Figure 2. SAXS intensity profiles from nylon 6,6 during (a) heating of the starting specimen and (b) cooling of the molten polymer.

Table 1

fit parameter	physical significance
a_1	intensity of the zero-angle scattering, I_D
a_2	an arbitrary size characterizing the zero-angle scattering
a_3	thickness of the interlamellar amorphous layer, l_a
a_4	intensity of the lamellar peak, I_L
a_5	lamellar spacing, L
a_6	coherence length of the lamellar stack, L_{coh}

for Gaussian peaks. The intensity, for comparison, can also be obtained as the invariant in the expression

$$Q = \int_0^\infty I(q)q^2 \, dq \tag{8}$$

In summary, six parameters whose physical significance is given in Table 1 completely describe the scattering between 0.02 and 0.2 Å^{-1}. A practical feature of the profile analysis is that it provides an L value that is corrected for the apparent shift in the lamellar peak maximum to higher q's due to the rapid decrease in the background intensity at higher q's. The calculation also takes into account the Lorentz factor that shifts the corrected peak to higher angles. Thus, for instance, a_5 = 0.062 Å^{-1} even though the apparent maxima in the raw data is at ~0.05 Å^{-1}. Equation 6 gives a value of L consistent with that obtained from correlation function analysis whereas a simple calculation from the peak maximum would give a much higher value.

The model described above is simplistic in that we assume that crystalline lamellae have sharp boundaries. Also, the effect of the variations in L, l_c, and l_a within a lamellar stack as well as in the assembly of lamellar stacks is lumped into a single parameter, a_6, that characterizes the width of the lamellar peak. A more realistic model requires the evaluation of additional parameters that cannot be reliably obtained from the data.

Results and Discussion

WAXD data obtained during these measurements are same as those that have been reported in many publications[16,18−24] and therefore will not be repeated here. Briefly, in the room temperature (22 °C) scans, there are two reflections at q = 1.47 and 1.72 Å^{-1}. As the temperature is increased, these peaks approach each other in q. A new peak at q = 1.52 Å^{-1} appears at ca. 100 °C. The intensity of this new peak increases gradually with temperature, and there is a concomitant decrease in the intensities of the two room temperature peaks. Above ca. 180 °C the 1.52 Å^{-1} is the only crystalline peak present; its intensity remains constant up to ca. 230 °C, and then it gradually decreases and disappears into an amorphous halo at 260 °C. The midpoint of the transformation from the two-peak pattern to the one-peak pattern, the Brill transition temperature (T_B), is ca. 160 °C.

Figure 2a,b shows the SAXS intensity profiles measured during heating and cooling. During heating, the scattering peak changes slowly at first and then more rapidly above 180 °C. These changes include a shift in the position of the lamellar peak to lower angles, sharpening of the peak, and an increase in peak intensity. The lamellar peak finally becomes a shoulder before disappearing in the melt. During cooling, the lamellar peak is not visible at temperatures above 240 °C and appears as a shoulder at 220 and 200 °C, and the peak is clearly present at 160 °C. The peak shifts to larger angles and becomes sharper and more intense as the melt is cooled. The scans in Figure 2 were analyzed by separating them into three components: I_B, I_D, and I_L (see "Data Analysis"). The background intensity I_B is not of much significance. The changes in the central diffuse scattering I_D are not relevant to the lamellar structure. We will therefore focus on the changes in intensity distribution of the lamellar peak, $I_L(q)$.

The changes in $I_L(q)$ as measured by the position of the lamellar peak (long period L), the height of the crystals (l_c), and the width of the interlamellar amorphous regions (l_a) are plotted as a function of temperature in Figure 3. L and l_c remain unchanged up to 200 °C and then increase rapidly above 220 °C, suggesting that the lamellae undergo large structural changes above 220 °C. This temperature is far above the Brill transition temperature of 160 °C (T_B), and the changes are similar to those reported for polymers such as PET,[28] PBT,[29] and PEEK[30] that do not exhibit a Brill transition. Thus, although WAXD data show that the crystalline phase undergoes a dramatic change at T_B during both heating and cooling,[24] no such change is seen in Figure 3 except for weak evidence that there might be some increase in l_a at about 160 °C during heating. It therefore appears that large changes in crystal structure at T_B do not affect the organization at the lamellar level. However, the changes in the coherence length of the lamellar stack (L_{coh}) and the integrated lamellar intensity (Figures 4 and 5) show that there are indeed significant changes in the lamellar structure that accompany the changes in the organization of the crystalline stems at the Brill transition temperature T_B. These changes, as in WAXD measurements, occur over a broad temperature range of 120−180 °C.

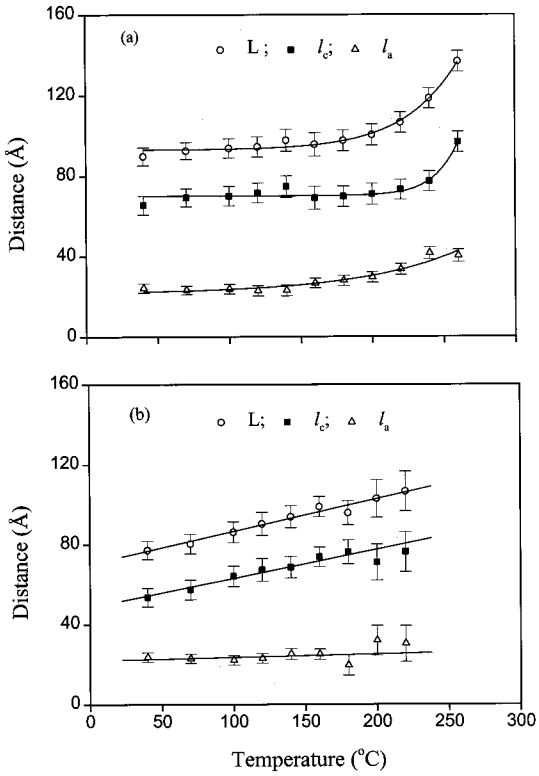

Figure 3. Morphological parameters of the lamellar structure (a) during heating and (b) during cooling. The long period (L), thickness of the interlamellar amorphous layer (l_a), and thickness of the crystalline lamellae ($l_c = L - l_a$) are shown at different temperatures.

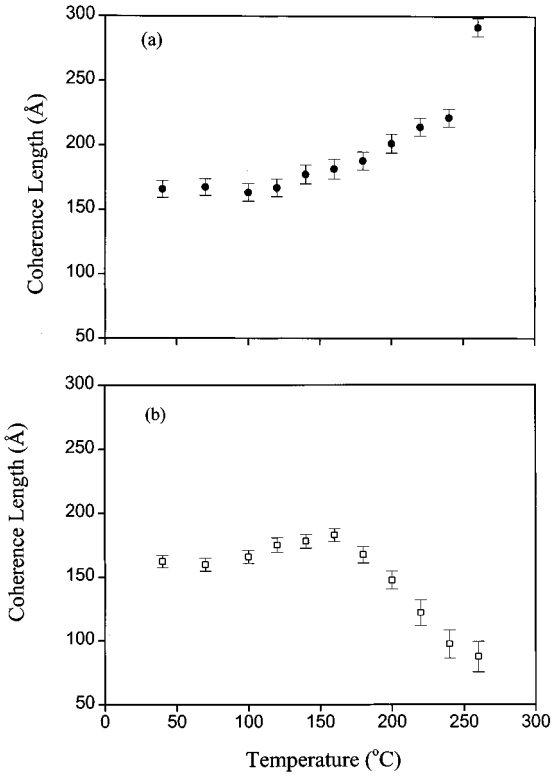

Figure 4. Variations in the coherence length of the lamellar stack as calculated from the parameter a_6: (a) during heating, (b) during cooling.

The increase in the coherence length of the lamellar stack during heating is normally attributed to melting of smaller lamellae. However, we see that the coherence length increases before there is any increase in the lamellar spacing (Figures 3 and 4). This suggests the increase in L_{coh} that we observe at 160 °C could be due to the elimination of the defects within the lamellar stacks. It is possible that the onset of librational motions of the crystalline stems at T_B,[19,20] releases microstrains, and defects such as kinks diffuse to the fold surface. The increase in the coherence length during cooling from T_m to T_B is caused by the decrease in the thermal vibrational motion of the crystalline stems. Further cooling below T_B apparently does not affect the coherence length of the lamellae that are already formed.

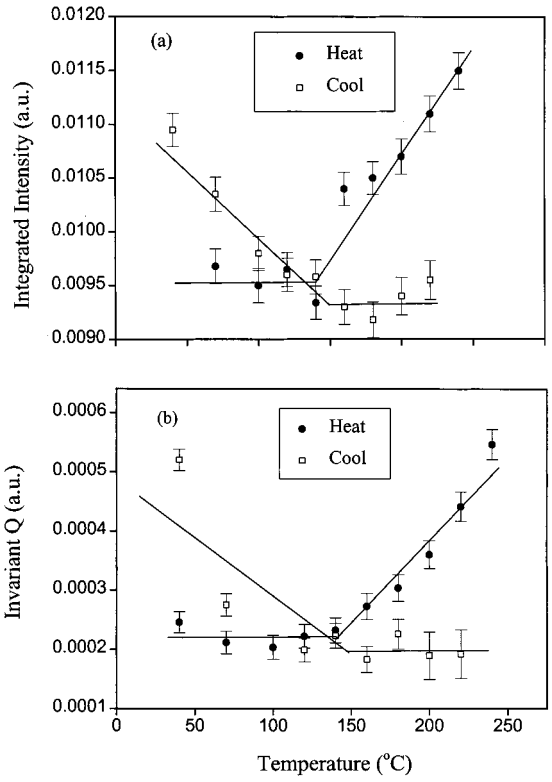

Figure 5. Variations in the lamellar peak intensity as derived from (a) the intensity profile analysis and (b) invariant calculations.

Figure 5 shows that there are large changes in the lamellar intensity according to both eqs 4 (profile analysis) and 8 (invariant). In polymers such as PEEK, which do not exhibit a Brill transition, the invariant decreases as the lamellar dimensions increase prior to melting.[30] In N66, during heating, the intensity of the lamellar peak initially remains unchanged up to about 140 °C and then begins to increase up until the melting of the lamellar crystals. These changes in intensity parallel the changes in the coherence length of the lamellar stack (Figure 4). On the other hand, the changes observed during cooling are quite different: the intensity remains unchanged from the melt to T_B and increases as the polymer is further cooled to room temperature. In contrast, the coherence length increases from T_m to T_B and then remains constant as the sample is further cooled.

The increase in the lamellar intensity is due to either or both an increase in the volume fraction of the crystalline lamellae or increase in the electron density contrast between the crystalline and the amorphous regions. Both of these factors contribute to the observed increase in the intensity during cooling. The volume fraction of the crystalline domains increases only after

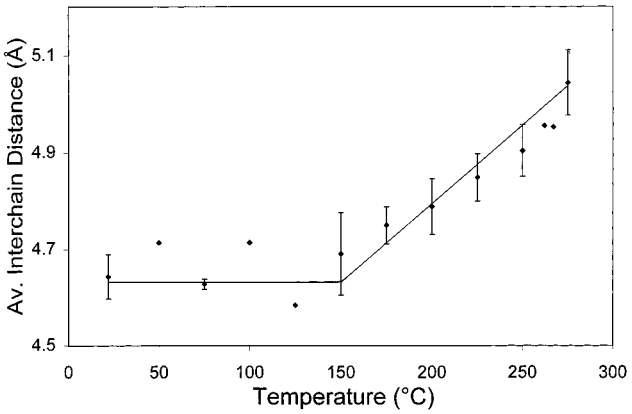

Figure 6. Plot of average interchain distance in the amorphous phase as a function of temperature during heating as calculated from the position of the amorphous halo. The error bars shown are the standard deviations calculated from four separate runs.

the melt is cooled below T_B. The density difference between the incipient crystals (which are in the pseudohexagonal form)[24] and the amorphous regions is small above T_B, and this contrast increases due to the increase in crystalline density as the polymer is cooled below T_B at which transformation into the room temperature triclinic phase sets in.

The interpretation of the observed increase in intensity during heating, however, is not as straightforward. The increase in intensity observed during heating above T_B is not due to an increase in the volume fraction of the crystallites because the crystallinity does not increase, and indeed may even decrease, during the Brill transition. The density of the high-temperature crystalline form is lower than the low-temperature crystalline (another triclinic) form. Therefore, the increase in contrast during heating is not due to an increase in crystalline density but has to be due to a decrease in the density of the amorphous phase. We speculate that the interlamellar amorphous chain segments are constrained at the fold surface, and as the crystalline stems rearrange at T_B, the amorphous chain segments become more mobile and thus less densely packed. The resulting increase in contrast could explain the dramatic increase in the SAXS intensity above T_B. Analysis of the previously published WAXD data[20] in fact suggests that the amorphous density does decrease at T_B during heating.

Figure 6 shows the results of analyses of the WAXD scans obtained at various temperatures in the form of average interchain distances (d) in the amorphous phase. The d values were calculated using the relation[34]

$$d = (7/2\pi)(\lambda/2 \sin \theta_{max}) = 1.11 d_{Bragg} \qquad (9)$$

where $2\theta_{max}$ is the position of the maximum in the amorphous halo and is the first and principal maximum in the Bessel function of zero order used to represent the scattering from bundles of parallel chain molecules. The amorphous halo is obtained by least-squares profile analysis of the WAXD scans as described in our earlier publications.[20,35] For polymers such as polyethylene and nylon, which do not have any side chains, it is reasonable to attribute the amorphous halo to interchain distances in the amorphous phase.[36,37] The figure shows that as the polymer is heated, the interchain distance initially remains essentially unchanged at 4.6−4.7 Å, increases rapidly above T_B, and reaches a value of 5 Å in the melt. Although one would expect the interchain distance to increase at all temperatures, the magnitude of this increase below T_B is probably within the sensitivity of our measurement and analysis. The increase in the amorphous interchain spacing above T_B corresponds to a decrease in the packing density of the chain segments in the amorphous phase. It is worth noting that such an increase in the average interchain distance in the amorphous phase with temperature was reported by Keller and co-workers.[24] However, they did not carry out a detailed analysis of the changes in the position of the amorphous halo similar to ours.

The slope of the least-squares fitted line at $T > T_B$ in Figure 6 is 0.0025 Å/K. This corresponds to a thermal expansion coefficient of 5.9×10^{-4}/K. This is similar to that for the crystalline regions reported by Itoh.[38] Assuming the length and diameter of a chain of monomer molecular weight 113 to be 8.5 and 4.25 Å, respectively, we calculate the molar thermal expansion coefficient ($\delta V/\delta T$) to be 854×10^{-10} m^3/(mol K) at $T > T_B$. This value is in reasonable agreement with the reported empirical value of 707×10^{-10} m^3/(mol K).[39] The acceleration of thermal expansion in the amorphous phase at T_B that we observe is consistent with an increase in the free volume. This allows large-amplitude motion in the amorphous domains as a result of the increased mobility of the chains in crystalline regions, especially at the crystal−amorphous interface. Thus, the density of packing of the amorphous chain segments is influenced by the arrangement of the crystalline stems within the lamellae.

Conclusion

Structural changes within the crystalline domains within the lamellae, such as the ones that occur during crystalline phase transitions, are accompanied by changes in the packing of the amorphous chain segments outside the lamellae. As a result, crystalline transitions, of which the Brill transition is an example, leave their signature in SAXS data. The observed changes in the integrated intensity during the Brill transition are attributed to the changes in the density of the interlamellar amorphous phase. The coherence length of the lamellar stacks also changes during this phase transition in nylon 6,6.

Acknowledgment. The authors acknowledge the financial support of this work by a grant from NSF (DMR 9732653). The authors also thank Dr. Fengji Yeh for his assistance during synchrotron experiments.

References and Notes

(1) Murthy, N. S.; Bray, R. G.; Correale, S. T.; Moore, R. A. F. *Polymer* **1995**, *36*, 3863.
(2) Murthy, N. S.; Bednarczyk, C.; Rim, P. B.; Nelson, C. J. *J. Appl. Polym. Sci.* **1997**, *64*, 1363.
(3) Hotter, J. F.; Cuculo, J. A.; Tucker, P. A.; Annis, B. K. *J. Appl. Polym. Sci.* **1998**, *69*, 2051.
(4) Hotter, J. F.; Cuculo, J. A.; Tucker, P. A.; Annis, B. K. *J. Appl. Polym. Sci.* **1998**, *69*, 2115.
(5) Wu, G.; Jiang, J.-D.; Tucker, P. A.; Cuculo, J. A. *J. Polym. Sci., Polym. Phys.* **1996**, *34*, 2035.
(6) Fu, Y.; Annis, B.; Boller, A.; Jin, Y.; Wunderlich, B. *J. Polym. Sci., Polym. Phys.* **1994**, *32*, 2289.
(7) Fu, Y. G.; Chen, W.; Pyda, M.; Londono, D.; Annis, B.; Boller, A.; Habenschuss, A.; Cheng, J. L.; Wunderlich, B. *J. Macromol. Sci., Phys.* **1996**, *B35* (1), 37.
(8) Chen, W.; Fu, Y. G.; Wunderlich, B.; Cheng, J. L. *J. Polym. Sci., Polym. Phys.* **1994**, *32*, 2661.
(9) Gupta, B. *J. Text. Inst.* **1995**, *86*, 299.

(10) Gohil, R. M. *J. Appl. Polym. Sci.* **1994**, *52*, 925.
(11) Murthy, N. S.; Bednarczyk, C.; Rim, P. B.; Nelson, C. J. *J. Appl. Polym. Sci.* **1997**, *64*, 1363.
(12) Rim, P. B.; Nelson, C. J. *J. Appl. Polym. Sci.* **1991**, *42*, 1807.
(13) Cheng, J. L.; Fone, M.; Reddy, V. L.; Schwartz, K. B.; Fisher, H. P.; Wunderlich, B. *J. Polym. Sci., Polym. Phys.* **1994**, *32*, 2683.
(14) Murthy, N. S.; Minor, H.; Latif, R. A. *J. Macromol. Sci., Phys.* **1987**, *B26*, 427.
(15) Murthy, N. S.; Stamm, M.; Sibilia, J. P.; Krimm, S. *Macromolecules* **1989**, *22*, 1261.
(16) Brill, R. *J. Prakt. Chem.* **1942**, *161*, 49.
(17) Starkweather, H. W., Jr. Transitions and Relaxations. In *Nylon Plastics Handbook*; Kohan, M. I., Ed.; Hanser: Munich, Germany 1995; p 139.
(18) Starkweather, H. W., Jr.; Jones, G. A. *J. Polym. Sci., Polym. Phys.* **1981**, *19*, 467.
(19) Hirschinger, J.; Miura, H.; Gardner, K. H.; English, A. D. *Macromolecules* **1990**, *23*, 2153.
(20) Murthy, N. S.; Curran, S. A.; Aharoni, S. M.; Minor, H. *Macromolecules* **1991**, *24*, 3215.
(21) Biangardi, H.-J. J. *Macromol. Sci., Phys.* **1990**, *B29*, 139.
(22) Radusch, M. J.; Stolp, M.; Androsch, A. *Polymer* **1994**, *35*, 3568.
(23) Xenopoulos, A.; Wunderlich, B. *Colloid. Polym. Sci.* **1991**, *269*, 375.
(24) Ramesh, C.; Keller, A.; Eltink, S. J. E. A. *Polymer* **1994**, *35*, 2483.
(25) Starkweather, H. W., Jr. *Macromolecules* **1989**, *22*, 2000.
(26) Vasanthan, N.; Murthy, N. S.; Bray, R. G. *Macromolecules* **1990**, *23*, 8433.
(27) Murthy, N. S.; Akkapeddi, M. K.; Orts, W. J. *Macromolecules* **1998**, *31*, 142.
(28) Wang, Z.-G.; Hsiao, B. S.; Bryan, B.; Sauer; William, G. K. *Polymer*, in press.
(29) Hsiao, B. S.; Wang, Z.-G.; Yeh, F.; Yan, G.; Sheth, K. C. *Polymer* **1999**, *40*, 3515.
(30) Verma, R. K.; Velikov, V.; Kander, R. G.; Marand, H.; Chu B.; Hsiao, B. S. *Polymer* **1996**, *37*, 5357.
(31) Wenig, W.; Bramer, R. *Colloid Polym. Sci.* **1978**, *256*, 125.
(32) Cameraon, R. E.; Donald, A. M. *Polymer* **1992**, *33*, 2628.
(33) Jenkins, P. J.; Donald, A. M. *Polymer* **1996**, *37*, 5559.
(34) Klug, H. P.; Alexander, L. E. *X-ray Diffraction Procedures*; Wiley: New York, 1974; p 849.
(35) Murthy, N. S.; Minor, H. *Polymer* **1990**, *31*, 996.
(36) Miller, R. L.; Boyer, R. F. *J. Polym. Sci., Polym. Phys.* **1984**, *22*, 2043.
(37) Murthy, N. S.; Minor, H.; Bednarczyk, C.; Krimm, S. *Macromolecules* **1993**, *26*, 1712.
(38) Itoh, T. *Jpn. J. Appl. Phys.* **1976**, *15*, 2295.
(39) Van Krevelen, D. W. *Properties of Polymers*; Elsevier: New York, 1976; pp 72−73.

MA990475E